Radiationless Decay of Excited States of Uracil through Conical Intersections

Spiridoula Matsika*

Department of Chemistry, Temple University, Philadelphia, Pennsylvania 19122

Received: April 20, 2004; In Final Form: July 6, 2004

The electronically excited singlet states of uracil have been studied theoretically using ab initio multireference configuration interaction methods focusing on the mechanism for radiationless decay back to the ground state. The first excited state with a significant oscillator strength is calculated to be the S_2 state, corresponding to an excitation $\pi \rightarrow \pi^*$, while a dark state, S_1 ($n_O \rightarrow \pi^*$), exists below S_2. Conical intersections have been located between the S_2 and S_1 states 0.9 eV below the vertical excitation to S_2 and between the S_1 and the ground state, ca. 1.8 eV below the vertical excitation energy to S_2. These conical intersections are connected with each other and the Franck Condon region by pathways that exhibit no barriers and provide for a nonradiative decay to the ground state.

1. Introduction

A detailed understanding of the properties and dynamics of the excited states of the DNA and RNA bases is very important because of their biological significance. These bases are the dominant chromophores in nucleic acids, and their photochemical and photophysical properties are implicated in the behavior of the nucleic acids upon irradiation. Absorption of solar ultraviolet (UV) radiation by the nucleic acids can lead to photochemical damage, so the photoinitiated processes taking place in the nucleobases may be an important component in DNA's photostability.

It has been known for years that the excited states of the nucleobases are short lived and that the quantum yields for fluorescence are very low.[1−3] Recent advances in experimental techniques have enabled the accurate measurement of their excited-state lifetimes.[4−19] Transient absorption spectroscopy[4−7] and fluorescence up-conversion techniques[8−11] have been used to measure the lifetimes and study the dynamics of nucleosides, nucleotides, and isolated bases, in solution. These studies report lifetimes on the order of femtoseconds and suggest that nonradiative relaxation proceeds on an ultrafast time scale to the ground state with the extra energy being transformed into heat.[4,5] Experiments in the gas phase have been performed as well, reporting spectra and lifetimes.[12−20] The lifetimes reported in many of these studies are also short, suggesting this to be an intrinsic property of the bases, but there are some studies that disagree and indicate that the mechanism for internal conversion in the gas phase differs from that in solution. He et al.[15,16] suggest a two-step mechanism where the first step occurs on an ultrafast time scale but the final decay to the ground state is slow because the system is trapped in a dark state for several nanoseconds. Thus the photophysical behavior of nucleobases in the gas phase compared to that in solution remains an open question, with specific information about the number of steps and efficiency of each step for the overall relaxation mechanism not being determined. Theoretical studies have contributed to the effort of elucidating the details of the radiationless decay mechanism.[21−25] Different methods have been used to calculate the excitation energies in nucleobases, ranging from semi-empirical to high-level ab initio methods.[24−34] The results vary significantly with the chosen method, making even the ordering of the states at vertical excitations ambiguous. Studying the photophysical properties imposes further difficulties since the gradients of the surfaces, in addition to the energies, are needed. The mechanism for nonradiative decay has been investigated for some isolated bases.[21−25] Detailed calculations have been done for cytosine addressing the involvement of conical intersections in the mechanism. A study using CASSCF methods to locate conical intersections[22] suggested a $\pi\pi^*-n_O\pi^*$ conical intersection followed by a $n_O\pi^*-S_0$ conical intersection, but another study, which used perturbative methods (CASPT2) to calculate the energies,[23] found the $\pi\pi^*$ state lower in energy and suggested only one conical intersection, $\pi\pi^*-S_0$, in the pathway. Thus, including dynamical correlation changed the details of the relaxation mechanism. A very different relaxation mechanism has been proposed for adenine involving conical intersections with a Rydberg state.[21] It should be noted that the above studies did not use methods with dynamical correlation to calculate the gradients and locate conical intersections.

Despite the experimental and theoretical efforts, the excited-state dynamics of the nucleobases remain poorly understood and further studies are needed to advance our knowledge in this area. In this work, we study the singlet excited states and relaxation pathways of uracil, using multireference configuration interaction (MRCI) methods. Analytic gradients and the location of conical intersections will be done at the correlated MRCI level. A recent study[7] shows uracil to be the pyrimidine base with the shortest fluorescence lifetime. The fluorescence lifetime of uridine in solution was measured to be 210 fs using transient absorption spectroscopy, with the decay time for uracil being very similar.[7] Here we focus on studying the mechanism for radiationless decay in uracil as a first step in understanding the radiationless decay in the nucleobases. Section 2 discusses the methods used for the electronic structure problem. In section 3, after a discussion on the states involved and their vertical excitation energies (section 3.1), results on conical intersections are presented (section 3.2). These conical intersections connect the relevant excited states with the ground state. Finally pathways connecting all these features are discussed in section 3.3, and conclusions are given in section 4.

* To whom correspondence may be addressed. E-mail: smatsika@temple.edu.

10.1021/jp048284n CCC: $27.50
Published on Web 08/19/2004

TABLE 1: Vertical Excitation Energies for the Four Lowest Excited States of Uracil[a]

	$S_1(A'')$	$S_2(A')$	$S_3(A'')$	$S_4(A')$
MRCI1(12,9)	5.44 (0.52×10^{-3})	6.24 (0.25)		
MRCI1(14,10)	5.45 (0.22×10^{-3})	6.23 (0.22)	6.89 ($<1 \times 10^{-6}$)	6.90 (0.051)
MRCI2(14,10)	5.55 (0.28×10^{-3})	6.29 (0.24)	7.03 ($<1 \times 10^{-6}$)	7.05 (0.055)
MRCI$\sigma\pi$	4.80 (0.15×10^{-3})	5.79 (0.19)	6.31 ($<1 \times 10^{-6}$)	6.57 (0.035)
CASSCF[b]	4.78	6.88	6.31	7.03
CASPT2[b]	4.54 (0.18×10^{-3})	5.00 (0.19)	6.00 (0.38×10^{-6})	5.82 (0.08)
DFT/MRCI[c]	4.61(0.00)	5.44 (0.26)	5.95 (0.00)	6.15 (0.050)
exp[d]		4.5−5.1		5.8−6.1

[a] Results from this work and other theoretical[30,34] and experimental[41,42] results are shown. All energies are in eV with the zero set to the energy of the ground state at $\mathbf{R}_e(S_0)$. Oscillator strengths are given in parentheses. [b] Reference 30. [c] Reference 34. [d] References 30, 41, 42.

2. Methods

The adiabatic energies and wave functions were determined at the MRCI level using orbitals from a state-averaged multiconfigurational self-consistent field (SA-MCSCF) procedure. The double-ζ plus polarization (cc-pvdz) Gaussian basis sets of Dunning were used for all atoms.[35] The molecular orbitals were obtained from a state-averaged CASSCF where three states were included in the average. Results reported in section 3.1, however, include five states in the average, rather than three, since excitation energies and oscillator strengths for four excited states, rather than two, were sought. The lowest excited states, if we neglect Rydberg states, originate from excitations from the valence π and lone pair n_O orbitals. In uracil there are eight π and two lone pair orbitals from the two oxygen atoms, thus the most appropriate active space in CASSCF should include these 10 orbitals, and a subsequent MRCI should have the same reference space, which generates 4 950 references. This active space, denoted (14,10), was used in this work for single-point calculations. The designation (*n*,*m*) is used here for an active space of *n* electrons in *m* orbitals. Two different MRCI expansions were generated from this active space. The first one included all single and double excitations from the (14,10) reference space consistent with the generalized interacting space restrictions.[36,37] It is denoted MRCI2 where 2 is used to indicate second-order MRCI. The interacting space restriction restricts the configuration state functions (CSFs) to those having a nonvanishing matrix element with one of the reference configurations. The remaining orbitals were always doubly occupied, and the resulting expansion consisted of ca. 175 million CSFs. This expansion, however, correlates only the valence π and *n* electrons and, as will be discussed further in the next section, is not able to reproduce accurate vertical excitation energies. For this, σ correlation should be included. The importance of correlating the σ electrons when describing $\pi\pi^*$ states is discussed by Borden and Davidson in a review article.[38] They have shown that a sum of double excitations of one core electron and one active electron from the HF wave function is important for a proper description of $\sigma-\pi$ polarization effects. An expansion with single excitations to all π configurations includes this correlation. In uracil, it is impossible to correlate all σ electrons with single and double excitations. An attempt to correlate the σ electrons including single and double excitations leads to expansions with a size of several billion CSFs making the corresponding calculations unattainable at present. So we had to compromise to an expansion that would at least include a measure of the $\sigma-\pi$ polarization effects. The reference configurations included the CAS in the (14,10) space as before plus configurations with single excitations from all σ electrons, except the 1s core, to the valence n,π space. Then all single excitations from the 227 865 generated configurations to all virtual orbitals were included. This expansion will be denoted MRCI$\sigma\pi$ in the following discussion, and consists of ca. 100 million CSFs. Results from this expansion are used to measure the effect of σ correlation on the energies. Since MRCI$\sigma\pi$ and MRCI2 include different correlation effects, results from both of them will be reported in the following discussion.

Optimizations and gradient-driven pathways cannot be carried out using either of these expansions, and a first-order expansion was used instead. The active space in this expansion, used in both the CASSCF and MRCI procedures, consisted of 12 electrons in 9 orbitals, denoted (12,9), where these 9 active orbitals were the 8 π and the 1 n_O valence orbitals. The expansion is denoted MRCI1 or MRCI1(12,9), where 1 indicates first-order MRCI. The active space will be included in the notation whenever there is a need to differentiate from expansions where the (14,10) active space is used. If the active space is not included, MRCI1 refers to MRCI1(12,9). The reduction of the active space from 10 to the above 9 orbitals reduced the size of the calculations significantly but it had almost no effect on the energies of the first three states when using a first-order expansion. This can be seen in Table 1 by comparing the vertical excitation energies of a first-order MRCI using the (12,9) active space (MRCI1(12,9)) with a first-order MRCI using the (14,10) active space (MRCI1(14,10)). If we were interested in the second $n_O\pi^*$ state, this (12,9) active space would not be sufficient since the second *n* orbital is not in the active space, but this does not present a problem here since the optimizations concern only the first three states. A first-order configuration interaction from the (12,9) active space generated 607 320 CSFs. Optimized geometries are usually easier to converge, and it is sufficient to use a lower-level method for obtaining minima, which is what we have done here. The adequacy of MRCI1(12,9) to obtain conical intersections is further tested by carrying out single-point calculations with the larger expansions, MRCI2 and MRCI$\sigma\pi$, to confirm that the two states remain close in energy at the higher level of calculations.

C_s symmetry was used only for the vertical excitations after the minimum of the ground state was confirmed to have planar symmetry, and all other calculations were carried out without any symmetry restrictions. The CASSCF and MRCI results were obtained using a modified version of the COLUMBUS suite of programs.[39] In this version, the algorithms for locating conical intersections[40] have been included.

3. Results and Discussion

3.1. Vertical and Adiabatic Excitation Energies. The structure of uracil is shown in Figure 1 with the labeling of the atoms that will be used throughout this paper to define its geometries. Geometries will be denoted by **R**. $\mathbf{R}_e(S_m)$ is the equilibrium geometry for state S_m. The primary goal of this work is to study the photophysics and relaxation pathways related to the first optically allowed state. In this section, the energies and

TABLE 2: Energies in eV for the Three Lowest States of Uracil at Optimized Geometries R[a]

	$\mathbf{R}_e(S_0)$	$\mathbf{R}_e(S_1)$	$\mathbf{R}_x(ci21)$	$\mathbf{R}_x(ci21p)$	$\mathbf{R}_x(ci10)$
S_0	**0**	1.18	2.15 (2.38,1.87)	0.86	**4.47**(4.39,3.96)
S_1	5.44 (5.55,4.80)	**4.35**(4.76,4.12)	**5.37**(5.55,4.83)	**5.72**	**4.47**(4.71,4.29)
S_2	6.24 (6.29,5.79)	5.86	**5.37**(5.66,4.88)	**5.72**	7.62

[a] The energies in bold in each column correspond to the state that was minimized. In the case of conical intersections, the energy is the minimized energy of the seam. MRCI1 results are shown (the zero is set to −412.624433 au). In parenthesis, the single-point energies obtained using MRCI2 (the zero is set to −412.775046 au) and MRCI$\sigma\pi$ (the zero is set to −412.815540 au) are reported as (MRCI2,MRCI$\sigma\pi$).

oscillator strengths for the five lowest states are presented so that the first optically allowed state could be identified. Since other theoretical and experimental results exist for the vertical transitions, they can be used to compare with the calculated energies. Our most important objective is to be confident about the qualitative picture presented here.

The ground-state minimum geometry has been obtained using the first-order CI expansion, MRCI1. The vertical excitation energies to the four lowest excited states have been calculated using the expansions, MRCI2 and MRCI$\sigma\pi$, at this geometry. These energies are reported in Table 1, where all the energies are given in eV and the minimum energy of the ground state is set to zero. The ground-state equilibrium geometry is planar, and the excited states at this geometry have A′ or A″ symmetry. The first excited state, S_1, has A″ symmetry corresponding to excitation from a lone pair oxygen orbital, n_{O^8}, to a π^* orbital. n_{O^8} is an n_O orbital on O^8 where the labeling of atoms is given in Figure 1. S_2 is an A′ state with $\pi\pi^*$ character. The next two states, S_3 and S_4, are close in energy, with S_3 being a A″($n_{O^7}\pi^*$) state and S_4 being a second A′($\pi\pi^*$) state.

The excited states of uracil have been studied theoretically previously with ab initio methods ranging from configuration interaction with single excitations (CIS)[26−28] to highly correlated CASPT2 methods,[30] MRCI methods,[32] and density functional approaches for excited states.[33,34] Table 1 reports vertical excitation energies using some of these methods.[30,34] A comparison of the different methods demonstrates the importance of incorporating dynamical correlation. The correlated methods MRCI, CASPT2, and DFT/MRCI agree in the ordering of the states with the exception that the S_3 and S_4 states are switched in CASPT2.

It is important to notice here the effect of the different MRCI expansions used for the excitation energies. Correlating the valence electrons by including single and double excitations from the n,π active space, as was done in MRCI2, is not adequate for accurate excitation energies. In fact this expansion of 175 CSFs does not improve the energies of the MRCI1(12,9) expansion at all, predicting them again about 1 eV too high compared to other methods and experimental values. Including σ polarization though even in the approximate way of MRCI$\sigma\pi$ improves the energies by 0.4−0.7 eV. This effect is present not only at vertical transitions but at the other points of interest in the potential-energy surface, conical intersections, and other minima, as will be seen in the other sections. The importance of σ correlation for obtaining accurate excitation energies in nucleobases has been addressed before by Roos et al.[30] by comparing CASSCF with CASPT2 excitation energies. As mentioned above, more generally the importance of σ dynamical correlation in $\pi\pi^*$ transitions has been discussed by Borden and Davidson.[38] In a review article, they give several examples where including all single excitations from all π configurations restores much of the dynamic electron correlation and gives much better excitation energies for $\pi\pi^*$ transitions. An approach of including single excitations from the σ core has been adopted recently by Boggio-Pasua et al.[43] Of course, we cannot recover all dynamic electron correlation since we cannot carry out the proper single and double excitations treatment. But MRCI$\sigma\pi$ allows us to show the importance of σ correlation across the potential-energy surface.

TABLE 3: Selected Internal Coordinates of the Optimized Geometries at Equilibrium Points and Minimum-Energy Points of Conical Intersection[a]

geometry	$\mathbf{R}_e(S_0)$	$\mathbf{R}_e(S_1)$	$\mathbf{R}_x(ci21)$	$\mathbf{R}_x(ci21p)$	$\mathbf{R}_x(ci10)$
$R(C^2N^3)$	1.374	1.384	1.365	1.335	1.367
$R(C^2N^1)$	1.373	1.362	1.401	1.410	1.430
$R(C^6N^1)$	1.371	1.402	1.351	1.330	1.321
$R(C^5C^6)$	1.350	1.424	1.484	1.511	1.435
$R(C^4N^3)$	1.396	1.385	1.431	1.462	1.435
$R(C^4C^5)$	1.462	1.357	1.387	1.415	1.495
$R(C^4O^8)$	1.199	1.343	1.248	1.205	1.191
$R(C^2O^7)$	1.200	1.202	1.201	1.216	1.193
$\angle O^7C^2N^1$	123	124	120	116	118
$\angle C^5C^6N^1$	121	117	114	114	119
$\angle C^4C^5C^6$	119	118	116	122	112
$\angle H^5C^5C^4$	119	121	119	119	101
$\angle O^8C^4N^3$	121	113	115	116	119
$\angle C^6C^5C^4H^6$	180	168	165	180	157
$\angle C^6C^5C^4H^5$	0	3	25	0	65

[a] Bond lengths are given in Å and angles in degrees. MRCI1 results are shown. More internal coordinates are given as supplemental information. The labeling of atoms is given in Figure 1.

Oscillator strengths are reported in Table 1 in parentheses. They do not depend on correlation as strongly as the excitation energies. As expected, the $\pi\pi^*$ state has a large oscillator strength and excitations corresponding to promoting a lone pair to a π^* orbital have small intensity. According to these results, a dark state exists below the optically allowed S_2 state. S_3 and S_4, being higher in energy than the lowest bright state S_2, will not be considered further, although they could be involved in the mechanism in an indirect way.

The adiabatic excitation energy for the S_1 state is reported in Table 2 and the optimized geometry in Table 3. The adiabatic energy is ca. 1 eV lower than the vertical excitation energy to S_1. The minimum was found in a geometry deviated from planarity. The bond lengths that change the most between the ground state and the excited state are the $R(C^4O^8)$ and $R(C^5C^6)$ bonds, which are elongated, and the $R(C^4C^5)$, which is shortened (Table 3). These changes are in accordance with an excitation from n_{O^8} to an antibonding π^* orbital. Although a minimum can be obtained for $S_2(\pi\pi^*)$ when restricted to C_s symmetry, this is only a saddle point and relaxing the symmetry restriction causes out-of-plane modes to reduce the energy further leading to a conical intersection. This will be discussed in more detail in the next section.

3.2. Conical Intersections. As was discussed in detail in section 3.1, and is shown in Table 1, among the lowest excited states in the UV area, $S_2(\pi\pi^*)$ is the first state with a significant oscillator strength. Absorption of UV light will populate this state, and a pathway for electronic relaxation back to the ground state will require two radiationless transitions. First a transition from S_2 to S_1 has to occur and then a transition from S_1 to the ground state. Conical intersections that can facilitate both of

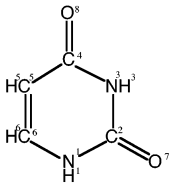

Figure 1. Molecular structure and labeling of the atoms in uracil.

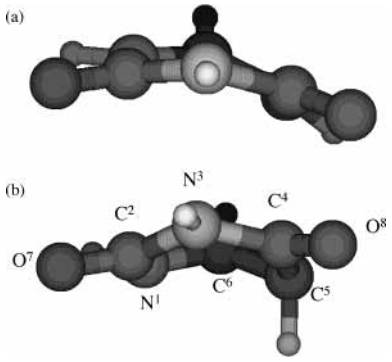

Figure 2. The geometry of uracil at (a) the S_1-S_2 conical intersection, *ci*21, and (b) the S_0-S_1 conical intersection, *ci*10.

these radiationless transitions were found and will be described here. An energy-minimized point of conical intersection between states S_m-S_n will be denoted *cimn*, and the geometry at this point $\mathbf{R}_x$(*cimn*). All gradient-driven calculations were done with the MRCI1 expansion, but single-point energy calculations at the minimum energy point of a seam were repeated using MRCI2 and MRCI$\sigma\pi$ to obtain the energies at the higher level of theory.

3.2.1. S_1-S_2 Conical Intersections. Points of conical intersection were found between the excited states S_1 and S_2 at energies lower than the vertical excitation energy to S_2. The seam of conical intersections contains both planar and nonplanar geometries. The minimum-energy point on the seam will be denoted *ci*21 and the point of conical intersection with planar symmetry *ci*21*p*. The energies and geometries at this point are given in Tables 2 and 3. Points on the seam that retain planar symmetry are 5.7 eV above the ground-state minimum energy at the MRCI1 level of theory, and the energy decreases from 5.7 to 5.4 eV when the structure deviates from planarity. The effect of the higher-level expansions MRCI2 and MRCI$\sigma\pi$ for the energies of S_1 and S_2 at $\mathbf{R}_x$(*ci*21) is similar to the effect observed for the vertical excitations. MRCI2 did not change these energies much, predicting 5.55 and 5.66 eV for S_1 and S_2, while MRCI$\sigma\pi$ dropped the energies by ca. 0.7 eV predicting them as 4.84 and 4.88 eV, respectively. At both $\mathbf{R}_x$(*ci*21*p*) and $\mathbf{R}_x$(*ci*21), the bond distances of the ring have changed indicating changes in the ordering of the bonds. At $\mathbf{R}_x$(*ci*21), R(C^5C^6) has increased from 1.35 to 1.48 Å, indicating a breaking of the corresponding double bond, while R(C^4C^5) has decreased from 1.46 to 1.39 Å. Furthermore, the breaking of planarity destabilizes the ground state by more than 1 eV, increasing its energy from 0.86 to 2.15 eV at the MRCI1 level, as shown in Table 2. The ring is deformed in a boat conformation where the two oxygen atoms have moved outside of the plane toward the same direction (see Figure 2 and Table 3).

3.2.2. S_0-S_1 Conical Intersections. A comparison of the energies at the two points of conical intersection *ci*21 and *ci*21*p* gives the first indication that breaking the planarity in uracil destabilizes the ground state but not the excited states. A systematic search located points of conical intersection between the ground state and S_1 at energies 4.47 eV above the minimum energy of the ground state at the MRCI1(12,9) level of theory. Again here MRCI2 does not affect the energies of the S_0 and S_1 states significantly as shown in Table 2, but MRCI$\sigma\pi$ lowers these energies giving 3.96 and 4.29 eV, respectively, with an average of 4.12 eV. At the intersection, the C^5H^5 bond is rotated outside of the plane, corresponding to a C^5 pyramidalization (Figure 2). The dihedral angle $\angle C^6C^5C^4H^5$, which shows how much H^5 deviates away from the plane of the carbon atoms, has increased to 65° at the minimum-energy point on this seam, compared to 25° at *ci*21. Another important point here is the character of the S_1 state. Although at the equilibrium geometries $\mathbf{R}_e(S_0)$ and $\mathbf{R}_e(S_1)$ the S_1 state corresponds to a $n_{O^8}\pi^*$ state, here it is the $\pi\pi^*$ state that has become lower in energy becoming the S_1 state that intersects with the ground state. The switch in character occurred during the S_1-S_2 conical intersections encountered before.

TABLE 4: Characteristic Parameters in au Describing the Topography of Conical Intersections *ci*10 and *ci*21

states	g	h	s_x	s_y
*ci*10	0.097	0.064	-0.066	0.028
*ci*21	0.15	0.035	0.051	0.0055

3.2.3. Topography of Conical Intersections. The topography of the potential-energy surfaces in the vicinity of a conical intersection plays a significant role in the efficacy of a conical intersection to promote a nonadiabatic transition.[40,44−47] This topography is described by nuclear displacements x and y along the branching plane,[44,48] a plane where the degeneracy of the states is lifted linearly. In uracil, the 30-dimensional nuclear coordinate space is divided into the two-dimensional branching space and the seam space of dimension $30 - 2 = 28$. The branching plane of a conical intersection between states I and J is spanned by the tuning and coupling vectors, $\mathbf{g}^{IJ}$ and $\mathbf{h}^{IJ}$, which correspond to the energy difference gradient and the coupling vector and are defined by[40]

$$2\mathbf{g}^{IJ}(\mathbf{R}) = \mathbf{c}^I(\mathbf{R}^x)[\nabla\mathbf{H}(\mathbf{R})]\mathbf{c}^I(\mathbf{R}^x) - \mathbf{c}^J(\mathbf{R}^x)[\nabla\mathbf{H}(\mathbf{R})]\mathbf{c}^J(\mathbf{R}^x) \quad (1)$$

$$\mathbf{h}^{IJ}(\mathbf{R}) = \mathbf{c}^I(\mathbf{R}^x)[\nabla\mathbf{H}(\mathbf{R})]\mathbf{c}^J(\mathbf{R}^x) \quad (2)$$

Here $\mathbf{c}^I$ are the expansion coefficients of the adiabatic wave functions $\Psi_I = \sum_{a=1}^{CSF} c_a^I\psi_a$ in the CSF basis and satisfy the equation $[\mathbf{H}(\mathbf{R}) - E_I(\mathbf{R})]\mathbf{c}^I(\mathbf{R}) = 0$, where $\mathbf{H}(\mathbf{R})$ is the electronic Hamiltonian in the CSF basis.[40]

The topography in the branching plane is given in terms of a set of parameters g, h, s_x, and s_y. The energies of the intersecting states I and J in terms of the above parameters are given by

$$E_{I,J}(x,y) = s_x x + s_y y \pm ((gx)^2 + (hy)^2)^{1/2} \quad (3)$$

where x and y are displacements along the $\mathbf{g}^{IJ}$ and $\mathbf{h}^{IJ}$ directions, respectively. The parameters g and h give the slope of the cone in the two directions $\mathbf{g}^{IJ}$ and $\mathbf{h}^{IJ}$, and the parameters s_x and s_y give the tilt of the cone.

The characteristic parameters for *ci*21 are shown in Table 4. The cone along the $\mathbf{g}^{IJ}$ direction is steep and tilted because of the large values of g and s_x, while along the $\mathbf{h}^{IJ}$ direction is very flat and vertical because of the small values of h and s_y. The derivative coupling and probability for nonadiabatic transitions are larger along the $\mathbf{h}^{IJ}$ direction,[49] but once the system is on the lower surface, the gradient is much steeper along the $\mathbf{g}^{IJ}$ direction. Nuclear dynamics in the vicinity of a conical intersection have confirmed that the topography affects the nuclear motion in this area.[46,47,50]

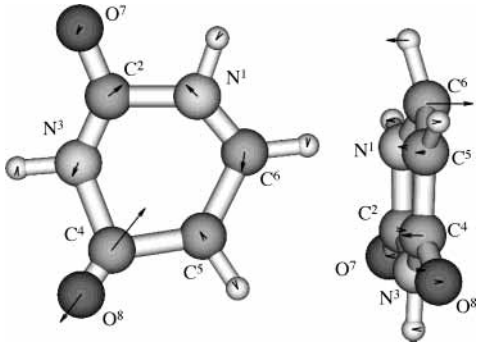

Figure 3. The $\mathbf{g}^{IJ}$ and $\mathbf{h}^{IJ}$ vectors for a point of conical intersection S_1-S_2 close to planar geometry in terms of atom centered Cartesian coordinates.

The $\mathbf{g}^{IJ}$ and $\mathbf{h}^{IJ}$ vectors represent nuclear displacements. At the planar symmetry points on the S_1-S_2 seam, the two states intersecting have different symmetries, (A′ and A″), so the $\mathbf{g}^{IJ}$ vector will be totally symmetric but the coupling vector $\mathbf{h}^{IJ}$ will have a″ symmetry and cause motion out of the plane. At the points of the seam where planarity is distorted, there is no A′ and A″ symmetry anymore, but the character of these two vectors does not change significantly. The two vectors at almost planar geometry are shown in Figure 3 in atom-centered Cartesian coordinates. $\mathbf{g}^{IJ}$ describes mainly an R(C^4O^8) stretching and $\mathbf{h}^{IJ}$ breaks the planar symmetry. Thus after going through the conical intersection *ci*21, the system can move along the $\mathbf{g}^{IJ}$ direction involving an R(C^4O^8) stretching or it can move along the $\mathbf{h}^{IJ}$ direction and continue breaking the planar symmetry. According to the characteristic parameters, the $\mathbf{g}^{IJ}$ direction has a steeper gradient. This information, taken here from the analysis at the point of conical intersection, is relevant to the possible pathways and overall photophysical behavior of uracil as will be discussed further below.

The topography of the conical intersection *ci*10 is described by the characteristic parameters shown in Table 4. The topography is more symmetric compared to the topography of the *ci*21 cone. The slopes are comparable in the two directions, and there is a small tilt in both directions. Both $\mathbf{g}^{IJ}$ and $\mathbf{h}^{IJ}$ vectors here involve bond stretching and bending.

3.3. Pathways. The minimum energy points for both *ci*10 and *ci*21 discussed in the previous section are at energies lower than the vertical excitation to S_2. These conical intersections provide the possibility for efficient radiationless decay to the ground state, provided there are pathways that connect the initial state (S_2 at vertical excitation) with the final state (ground state) through the conical intersections without, or with small, energy barriers. The next step then is to examine whether these pathways exist. To this aim, we carried out gradient-driven pathway calculations where the energy gradient was followed on one of the potential-energy surfaces.

Gradient-Directed Path from S_2 to *ci*21. Immediately upon excitation to the $S_2(\pi\pi^*)$ state, the system will evolve on that surface. The gradient of the S_2 surface was followed, and this pathway led directly to the *ci*21 conical intersection without any barrier. Figure 4 shows this gradient-directed path from the Franck Condon region to the *ci*21 conical intersection along the dihedral angle $\angle C^6C^5C^4H^5$. During the first steps of the gradient-directed path, the bond distance R(C^4C^5) increases from 1.35 to 1.48 Å and that change brings the two states close in energy. After the initial steps, R(C^4C^5) does not change substantially anymore while the dihedral angle $\angle C^6C^5C^4H^5$ continues to change, and this change decreases the energy of the seam of conical intersections S_2-S_1 and increases the energy

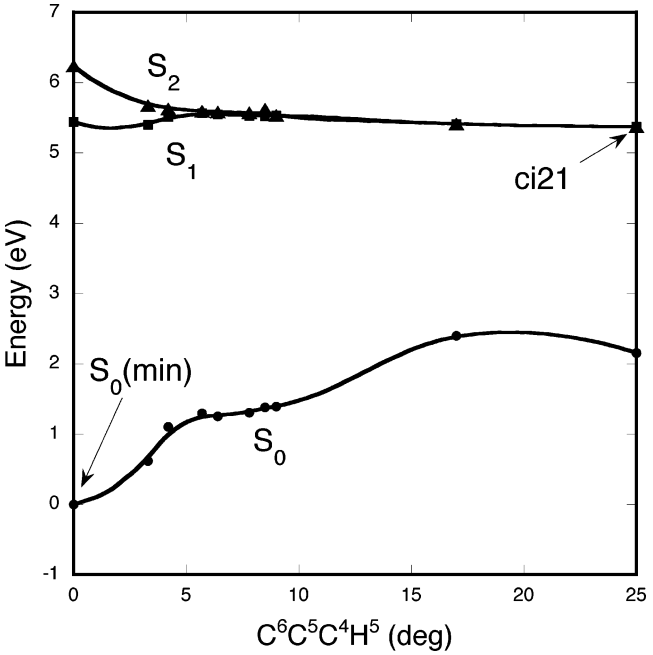

Figure 4. Gradient-directed pathway from the equilibrium geometry of the ground state, following the gradient of the S_2 surface, which leads to *ci*21. The energies of the S_0, S_1, and S_2 states relative to the minimum of S_0 are plotted as a function of the dihedral angle $\angle C^6C^5C^4H^5$.

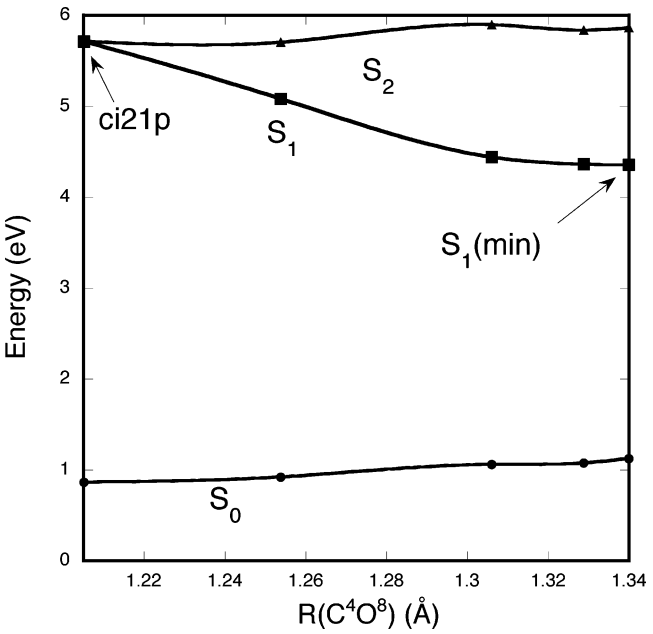

Figure 5. Gradient-directed pathway from a displacement along the $\mathbf{g}^{IJ}$ direction of the planar conical intersection *ci*21*p*, following the gradient on the S_1 surface, which leads to the S_1 minimum. The energies of the S_0, S_1, and S_2 states relative to the minimum of S_0 are plotted along R(C^4O^8).

of S_0. This approaching of the S_0 surface is important for the subsequent evolution of the system.

Gradient-Directed Paths from *ci*21. After the conical intersection *ci*21 is encountered, the system can emerge to the lower surface S_1. To examine the possible pathways after this nonadiabatic transition, we followed the gradient on the lower surface, S_1, starting from points displaced along the $\mathbf{g}^{IJ}$ or $\mathbf{h}^{IJ}$ coordinates.

Figure 5 shows a gradient-directed path starting from a point displaced from *ci*21*p* along the $\mathbf{g}^{IJ}$ direction. The path leads to

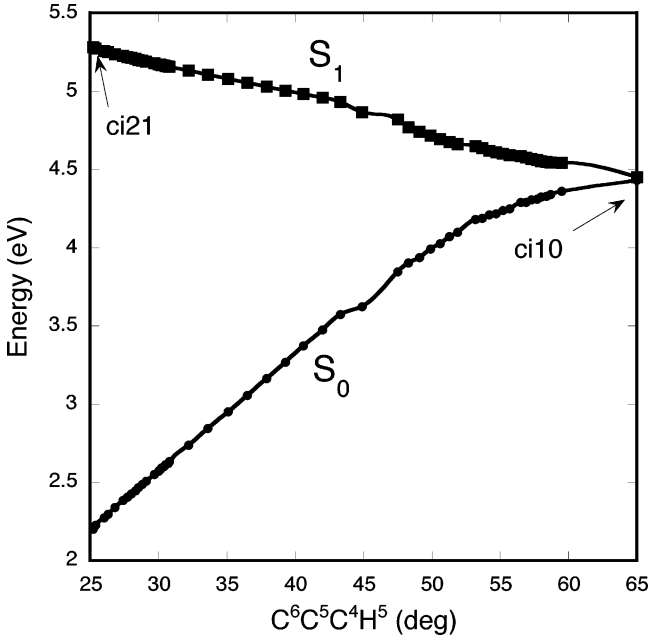

Figure 6. Gradient-directed pathway from *ci*21 connecting *ci*21 to *ci*10. The energies of the S_1 and S_0 states relative to the minimum of S_0 are plotted along the dihedral angle $\angle C^6C^5C^4H^5$.

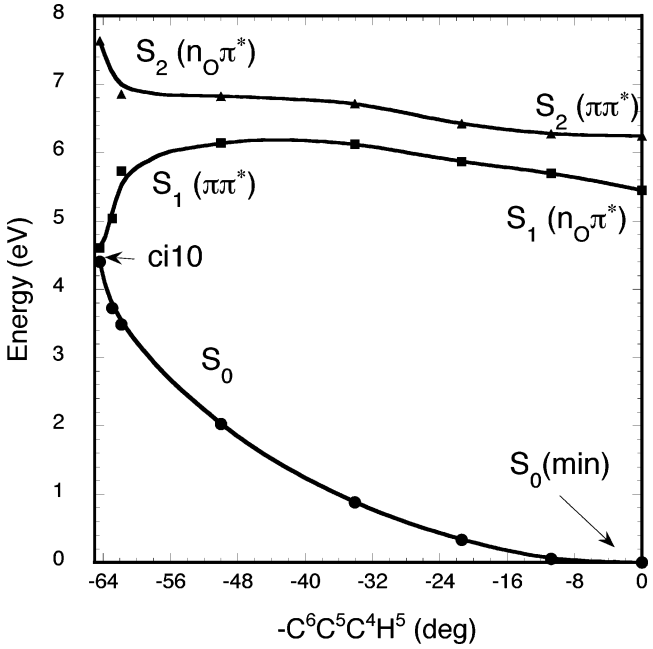

Figure 7. Gradient-directed pathway from a displacement along the $\mathbf{g}^{IJ}$ direction of the conical intersection *ci*10, following the gradient of the S_0 surface, which leads to the S_0 minimum. The energies of the S_0, S_1, and S_2 states relative to the minimum of S_0 are plotted along $\angle C^6C^5C^4H^5$.

the minimum of the S_1 surface. The main internal coordinate involved is the $R(C^4O^8)$, and the energies of the S_0, S_1, and S_2 states along this coordinate are shown in Figure 5. This pathway shows the system evolving to the minimum of the dark state S_1 where it could be trapped before having the chance to decay to the ground state. This possibility has been suggested by experimental work in the gas phase.[15,16] Simple inspection of the $\mathbf{g}^{IJ}$ displacements, as shown in Figure 3, could help us predict that the pathway would evolve mainly along the $R(C^4O^8)$ coordinate. This is a demonstration of the advantage of obtaining the $\mathbf{g}^{IJ}$ and $\mathbf{h}^{IJ}$ vectors at the conical intersection. These vectors give information about the possible outcome after encountering the conical intersection.

Alternatively, the system may reach the *ci*10 conical intersection, which will enable fast radiationless transition to the ground state. Starting from a displacement from *ci*21, the *ci*10 can be reached as shown in Figure 6. After the encounter with *ci*21, the lower surface S_1 will have either $n_{O^8}\pi^*$ or $\pi\pi^*$ character. If the initial point has $\pi\pi^*$ character, the gradient-directed path will lead to *ci*10. The energies of the S_1 and S_0 states along this path are shown in Figure 6. So, the seam of conical intersections between S_0-S_1 can be reached from *ci*21, and the pathway involves the H^5 moving away from the plane, depicted by the dihedral angle $\angle C^6C^5C^4H^5$.

In summary, pathways from *ci*21 along the S_1 surface give two possibilities: either the system can evolve to the minimum of that surface or a conical intersection with the ground state can be reached. The competition between the different pathways will determine the efficiency for radiationless decay to the ground state. The calculations presented here cannot determine the outcome of this competition, which can only be determined if nuclear motion is taken into account.

Gradient-Directed Path from *ci*10. Figure 7 shows a gradient-directed pathway from the vicinity of *ci*10 to the ground-state minimum following the gradient on the S_0 surface. The energies of all three relevant states along the dihedral angle $\angle C^6C^5C^4H^5$ are shown. A very interesting point is the character of the S_1 state along this pathway. As was discussed in section 3.2, at *ci*10 (initial point of the pathway), the character of S_1 is $\pi\pi^*$ while at $\mathbf{R}_e(S_0)$ (final point) is $n_{O^8}\pi^*$. Thus, there is a switch in the character along the pathway, caused by avoided crossing between S_1 and S_2. Figure 7 summarizes the behavior of the three surfaces along the dihedral angle $\angle C^6C^5C^4H^5$. Starting from $\angle C^6C^5C^4H^5 = 0$ at the Franck Condon region, an increase of this angle first brings the S_2-S_1 states together and further increase brings the S_1-S_0 states together.

4. Conclusions

The electronic relaxation mechanism of the excited states of uracil has been studied using MRCI ab initio methods focusing on the involvement of conical intersections. The lowest excited states are $S_1(n_{O^8}\pi^*)$, $S_2(\pi\pi^*)$, $S_3(n_{O^7}\pi^*)$, and $S_4(\pi\pi^*)$ with S_2 having the strongest oscillator strength. Conical intersections have been located connecting S_2 with S_1 and S_1 with the ground state. The conical intersections between S_2 and S_1 are easily accessible from the Franck Condon region at energies 4.83 eV at the MRCI$\sigma\pi$ level (5.3 eV at MRCI1 level). The geometry changes involve mainly the C^5C^6 bond stretching and the C^4C^5 bond contracting. The seam of conical intersections between S_2 and S_1 contains points with both planar and nonplanar geometries. A gradient-minimized pathway from the planar conical intersection, *ci*21*p*, leads to the minimum of the S_1 surface. Another pathway, however, leads to conical intersections between S_1 and S_0. *ci*10 is located ca. 4.12 eV above the minimum of the ground state at the MRCI$\sigma\pi$ level of theory (4.47 eV at the MRCI1 level) and has a nonplanar geometry with the C^5H^5 bond rotated out of the initial molecular plane and almost perpendicular to it (see Figure 2).

The above conical intersections provide pathways for fast radiationless decay to the ground state. The calculations also provide the alternative possibility, proposed by experimental work in the gas phase, that, after the initial S_2-S_1 decay, the system is trapped into the dark state S_1. The competition between the different pathways will determine the efficiency and overall rate for radiationless decay to the ground state.

It is interesting to compare the results reported here with the previously published results on cytosine.[22,23] As was discussed in the Introduction, the two studies published do not agree on the ordering of the states and the conical intersections involved. Nevertheless, both studies agree that the pathway involves a CO bond stretching followed by out of plane modes of the hydrogen substituent (carbon pyramidalization). The states involved in the relaxation of excited states in uracil are different from the ones in cytosine. Although an $n_O\pi^*$ is present in both cases, in uracil, we found the $n_{O^8}\pi^*$ excited state being involved while in cytosine it is the equivalent to the $n_{O^7}\pi^*$. In both molecules, the relaxation involves bond stretching followed by out of plane modes of the hydrogen substituent (carbon pyramidalization). But because of the different oxygen lone pairs involved, in cytosine, H^6 is the hydrogen atom involved, while in uracil, we found H^5 being the primary atom breaking the symmetry. In the third pyrimidine base, thymine, H^5 is substituted by a methyl group. It will be interesting to see the effect of this substitution on the details of the above mechanism, especially since H^5 participates in the most important coordinate for the mechanism reported here.

In this study, we focused on singlet excited states of uracil in the gas phase. Triplet states, as well as Rydberg states, were not considered. As other ab initio calculations have shown, triplet states exist below the singlet states discussed here, but any coupling of the ground state (which is a singlet) with these states is much smaller than coupling with singlet states. If a very efficient coupling mechanism can exist in the singlet manifold of states as seen here, the singlet−triplet contribution to such a mechanism should be small. The contribution of Rydberg states on a radiationless decay mechanism for uracil should not be direct since these states are located higher in energy than the bright S_2 state. This does not exclude the possibility that Rydberg states may contribute in some pathway for radiationless decay. Finally, the effect of the solvent has been neglected in this work, but is expected to play a major role when comparing the solution with the gas-phase experiments. This effect is one of the crucial questions in understanding the mechanism for radiationless decay. The solvent shifts the energy levels but not in the same way. Transitions to $n_O\pi^*$ states are blue shifted much more than transitions to $\pi\pi^*$ states. These shifts may change the ordering of the states and alter the potential landscape. Calculations in uracil have shown that hydration does change the ordering of S_1 and S_2 states, bringing the $\pi\pi^*$ state lower than the $n\pi^*$ only by 0.05 eV.[27,34] This switch may have important consequences for the proposed mechanism. In this work, solvent effects have been neglected, but in the future, solvation models will be used to add the effect of the solvent.

Acknowledgment. Financial support was provided by Temple University. David R. Yarkony is gratefully acknowledged for providing computer time at his laboratory's IBM RS6000 workstations.

Supporting Information Available: Additional internal coordinates of the optimized geometries. This material is available free of charge via the Internet at http://pubs.acs.org.

References and Notes

(1) Daniels, M.; Hauswirth, W. *Science* **1971**, *171*, 675.
(2) Daniels, M. In *Photochemistry and Photobiology of Nucleic Acids*; Wang, S. Y., Ed.; Academic Press: New York, 1976; Vol. 1, p 23.
(3) Callis, P. R. *Annu. Rev. Phys. Chem.* **1983**, *34*, 329.
(4) Pecourt, J.-M. L.; Peon, J.; Kohler, B. *J. Am. Chem. Soc.* **2000**, *122*, 9348−9349.
(5) Pecourt, J.-M. L.; Peon, J.; Kohler, B. *J. Am. Chem. Soc.* **2001**, *123*, 10370−10378.
(6) Cohen, B.; Hare, P.; Kohler, B. *J. Am. Chem. Soc.* **2003**, *125*, 13594−13601.
(7) Cohen, B.; Crespo-Hernandez, C. E.; Kohler, B. *Faraday Discuss.* **2004**, *127*, 000.
(8) Peon, J.; Zewail, A. H. *Chem. Phys. Lett.* **2001**, *348*, 255−262.
(9) Gustavsson, T.; Sharonov, A.; Markovitsi, D. *Chem. Phys. Lett.* **2002**, *351*, 195−200.
(10) Gustavsson, T.; Sharonov, A.; Onidas, D.; Markovitsi, D. *Chem. Phys. Lett.* **2002**, *356*, 49.
(11) Onidas, D.; Markovitsi, D.; Marguet, S.; Sharonov, A.; Gustavsson, T. *J. Phys. Chem. B* **2002**, *106*, 11367.
(12) Nir, E.; Kleinermanns, K.; Grace, L.; de Vries, M. S. *J. Phys. Chem. A* **2001**, *105*, 5106−5110.
(13) Piuzzi, F.; Mons, M.; Dimicoli, I.; Tardivel, B.; Zhao, Q. *Chem. Phys.* **2001**, *270*, 205−214.
(14) Lührs, D. C.; Viallon, J.; Fischer, I. *PCCP* **2001**, *3*, 1827.
(15) He, Y.; Wu, C.; Kong, W. *J. Phys. Chem. A* **2003**, *107*, 5145−5148.
(16) He, Y.; Wu, C.; Kong, W. *J. Phys. Chem. A* **2004**, *108*, 943−949.
(17) Kang, H.; Lee, K. T.; Jung, B.; Ko, Y. J.; Kim, S. K. *J. Am. Chem. Soc.* **2002**, *124*, 12958.
(18) Kang, H.; Jung, B.; Kim, S. K. *J. Chem. Phys.* **2003**, *118*, 6717.
(19) Ullrich, S.; Schultz, T.; Zgierski, M. Z.; Stolow, A. *J. Am. Chem. Soc.* **2004**, *126*, 2262.
(20) Brady, B. B.; Peteanu, L.; Levy, D. H. *Chem. Phys. Lett.* **1988**, *147*, 538−543.
(21) Sobolewski, A. L.; Domcke, W. *Eur. Phys. J. D* **2002**, *20*, 369−374.
(22) Ismail, N.; Blancafort, L.; Olivucci, M.; Kohler, B.; Robb, M. A. *J. Am. Chem. Soc.* **2002**, *124*, 6818−6819.
(23) Merchán, M.; Serrano-Andrés, L. *J. Am. Chem. Soc.* **2003**, *125*, 8108−8109.
(24) Broo, A. *J. Phys. Chem. A* **1998**, *102*, 526.
(25) Mennucci, B.; Toniolo, A.; Tomasi, J. *J. Phys. Chem. A* **2001**, *105*, 4749−4757.
(26) Broo, A.; Holmén. *J. Phys. Chem. A* **1997**, *101*, 3589.
(27) Shukla, M. K.; Leszczynski, J. *J. Phys. Chem. A* **2002**, *106*, 8642.
(28) Shukla, M. K.; Mishra, P. C. *Chem. Phys.* **1999**, *240*, 319.
(29) Mishra, S. K.; Shukla, M. K.; Mishra, P. C. *Spectrochim. Acta A* **2000**, *56*, 1355.
(30) Lorentzon, J.; Fülscher, M. P.; Roos, B. O. *J. Am. Chem. Soc.* **1995**, *117*, 9265−9273.
(31) Salter, L. M.; Chaban, G. M. *J. Phys. Chem. A* **2002**, *106*, 4251.
(32) Petke, J. D.; Maggiora, G. M.; Christoffersen, R. E. *J. Phys. Chem.* **1992**, *96*, 6992−7001.
(33) Neiss, C.; Saalfrank, P.; Parac, M.; Grimme, S. *J. Phys. Chem. A* **2003**, *107*, 140.
(34) Marian, C. M.; Schneider, F.; Kleinschmidt, M.; Tatchen, J. *Eur. Phys. J. D* **2002**, *20*, 357−367.
(35) Dunning, T. H. *J. Chem. Phys.* **1970**, *53*, 2823.
(36) McLean, A.; Liu, B. *J. Chem. Phys.* **1973**, *58*, 1066.
(37) Bunge, A. *J. Chem. Phys.* **1970**, *53*, 20.
(38) Borden, W. T.; Davidson, E. R. *Acc. Chem. Res.* **1996**, *29*, 67.
(39) A progress report on the status of the COLUMBUS MR-CI program system. Lischka, H.; Shepard, R.; Shavitt, I.; Pitzer, R. M.; Dallos, M.; Mller, T.; Szalay, P. G.; Brown, F. B.; Ahlrichs, R.; Bhm, H. J.; Chang, A.; Comeau, D. C.; Gdanitz, R.; Dachsel, H.; Ehrhardt, C.; Ernzerhof, M.; Hchtl, P.; Irle, S.; Kedziora, G.; Kovar, T.; Parasuk, V.; Pepper, M. J. M.; Scharf, P.; Schiffer, H.; Schindler, M.; Schler, M.; Seth, M.; Stahlberg, E. A.; Zhao, J.-G.; Yabushita, S.; Zhang, Z.
(40) Yarkony, D. R. *J. Phys. Chem. A* **2001**, *105*, 6277−6293.
(41) Clark, L. B.; Peschel, G. G.; Tinoco, I., Jr. *J. Phys. Chem.* **1965**, *69*, 3615.
(42) Clark, L. B.; Tinoco, I., Jr. *J. Am. Chem. Soc.* **1965**, *87*, 11.
(43) Boggio-Pasqua, M.; Bearpark, M. J.; Klene, M.; Robb, M. A. *J. Chem. Phys.* **2004**, *120*, 7849.
(44) Atchity, G. J.; Xantheas, S. S.; Ruedenberg, K. *J. Chem. Phys.* **1991**, *95*, 1862.
(45) Ben-Nun, M.; Molnar, F.; Schulten, K.; Martinez, T. J. *Proc. Natl. Acad. Sci. U. S. A.* **2000**, *97*, 9379−9384.
(46) Köppel, H.; Domcke, W.; Cederbaum, L. S. *Adv. Chem. Phys.* **1984**, *57*, 59−246.
(47) Domcke, W.; Stock, G. *Adv. Chem. Phys.* **1997**, *100*, 1−170.
(48) Yarkony, D. R. *Acc. Chem. Res.* **1998**, *31*, 511−518.
(49) Matsika, S.; Yarkony, D. R. *J. Phys. Chem. A* **2002**, *106*, 2580−2591.
(50) Yarkony, D. R. *J. Chem. Phys.* **2001**, *114*, 2601−2613.